

International Conference on Space Optics—ICSO 2020

Virtual Conference

30 March–2 April 2021

Edited by Bruno Cugny, Zoran Sodnik, and Nikos Karafolas



FCI PFM optical test results



FCI PFM optical test results

Julien Ouaknine*^a, Catherine Gaudin-Delrieu^a, Arnaud Liotard^a
Alessandro Boni^b, Donny Aminou^c, Yannig Durand^c

^aThales Alenia Space, 5 allée des Gabians, 06150 Cannes-La-Bocca, France; ^bOHB System AG, Manfred-Fuchs-Str. 1, D-82234 Weßling, Germany; ^cESTEC, Keplerlaan 1, 2201 Noordwijk, NL

ABSTRACT

Meteosat Third Generation is the next ESA Program of Earth Observation dedicated to accurate prediction of meteorological phenomena and climate monitoring. The satellites will be operating from the Geostationary orbit using a 3-axes stabilized platform. The main instrument is called the Flexible Combined Imager (FCI), currently under development by Thales Alenia Space France, the PFM being integrated and tested in our Cannes facilities. This instrument will provide full images of the Earth every 10 minutes in 16 spectral channels between 0.44 and 13.3 μm , with a ground resolution ranging from 0.5 km to 2 km. The FCI is composed of a Korsch telescope developed by OHB, followed by an assembly of lenses and detectors called the Spectral Separation and Detection Assembly (SSDA) which is integrated by Thales Alenia Space. Both the telescope and SSDA have been separately tested as sub-systems before being integrated. This article will describe the principle and results of the optical tests performed on these sub-systems. In particular the telescope WFE, focal length and line of sight have been proved to be compliant to the respective success criteria. Concerning the SSDA, we will present the results of MTF measurements, co-registration between spectral channels and polarization, which were also all found compliant to their respective success criterion. Stray-light for both the telescope and SSDA has been characterized on-ground in order to provide the input necessary for the development of image correction algorithms. During the first half of 2020, these two successfully tested sub-systems were integrated together to build the FCI PFM, which will undergo optical vacuum testing at the timeframe of beginning 2021 before being delivered to the satellite.

Keywords: FCI, optical, tests, meteorology

1. FCI MISSION OBJECTIVES AND OPTICAL DESIGN

We will first recall briefly the main system objectives of the FCI mission.

1.1 Introduction

The MTG program will provide the international community with meteorological and weather forecast data. It consists of two missions with distinct satellites : the imager mission named MTG-I, and the sounding mission named MTG-S. The FCI instrument will be mounted on the MTG-I satellites, 4 of them being ordered by ESA, to perform the continuation of service of the MSG mission. The satellites will be operating from a Geostationary orbit above Europe and Africa, using a 3-axes stabilized platform. The FCI is currently under development by Thales Alenia Space, which is the instrument prime contractor, with OHB as the main sub-contractor in charge of the telescope development. The development logic of the instrument is presented in [3].

1.2 Spectral and spatial resolution

The FCI will produce images of the Earth simultaneously in 16 spectral channels, ranging from the visible spectrum to thermal infra-red, in order to fulfill the scientific needs. The central wavelengths and spectral widths (FWHM) are illustrated in Table 1. The spectral channels are separated in 5 groups named VIS, NIR, IR1, IR2, and IR3. The on-ground spatial sampling distance (SSD) of the instrument is also given in Table 1 below. When two values are indicated in the spatial sampling distance column, it means that the spectral channel product can be delivered both in low and high resolution, thanks to the binning of adjacent pixels signals performed by post-processing. The FCI paraxial characteristics, such as focal length, pupil diameter and instantaneous field of view for each spectral group, are given in section 1.3.

*julien.ouaknine@thalesaleniaspace.com

Table 1. FCI spectral channels definition and corresponding on-ground spatial sampling

| Spectral Channel | Central Wavelength, λ_0 (μm) | Spectral Width, FWHM (μm) | On-ground spatial sampling distance (km) |
|------------------|---|--|--|
| VIS 0.4 | 0.444 | 0.060 | 1.0 |
| VIS 0.5 | 0.510 | 0.040 | 1.0 |
| VIS 0.6 | 0.640 | 0.050 | 1.0 / 0.5 |
| VIS 0.8 | 0.865 | 0.050 | 1.0 |
| VIS 0.9 | 0.914 | 0.020 | 1.0 |
| NIR 1.3 | 1.380 | 0.030 | 1.0 |
| NIR 1.6 | 1.610 | 0.050 | 1.0 |
| NIR 2.2 | 2.250 | 0.050 | 1.0 / 0.5 |
| IR1 3.8 | 3.800 | 0.400 | 2.0 / 1.0 |
| IR1 6.3 | 6.300 | 1.000 | 2.0 |
| IR1 7.3 | 7.350 | 0.500 | 2.0 |
| IR2 8.7 | 8.700 | 0.400 | 2.0 |
| IR2 9.7 | 9.660 | 0.300 | 2.0 |
| IR3 10.5 | 10.500 | 0.700 | 2.0 / 1.0 |
| IR3 12.3 | 12.300 | 0.500 | 2.0 |
| IR3 13.3 | 13.300 | 0.600 | 2.0 |

1.3 Paraxial characteristics

The following table gives the optical paraxial characteristics of the instrument, as a result of the mission needs.

Table 2. FCI optical paraxial characteristics

| | VIS | NIR | IR1 | IR2 | IR3 |
|--|-----------|-----------|-----------|-----------|-----------|
| Paraxial focal length (mm) | 1650 | 890 | 450 | 450 | 450 |
| Entrance pupil diameter (mm) | 300 | 300 | 300 | 300 | 300 |
| Instantaneous field of view N/S*E/W ($^\circ$) | 0.40*0.40 | 0.40*0.40 | 0.40*0.74 | 0.40*0.74 | 0.40*0.74 |

1.4 Instrument optical architecture

For a detailed presentation of the FCI optical design, refer to [1]. The FCI is composed of the following optical sub-systems :

- First, it is constituted by a three mirror anastigmat telescope, with a double-gimbaled flat mirror named M0 that scans the full Earth. The light-weighted mirrors are made of Zerodur (except M0 in SiC) with space-qualified silver protected coatings. The stiffness of the Invar Mirror Fixation Devices has been optimized to avoid generating deformation on the mirror surface from interface tolerances. The optical bench is made of aluminium nida with CFRP sandwich panels (Carbon Fiber Re-enforced Polymer), to minimize the thermal dilatation of the structure. The WFE after alignment of the telescope should be lower than 100 nm rms. The entrance pupil of the telescope is on the scan mirror to minimize its size. The telescope exhibits an intermediate image that allows to insert calibration devices such as an embedded black-body. The beam coming from the Earth is focused in the telescope focal plane and then reaches the following sub-system.

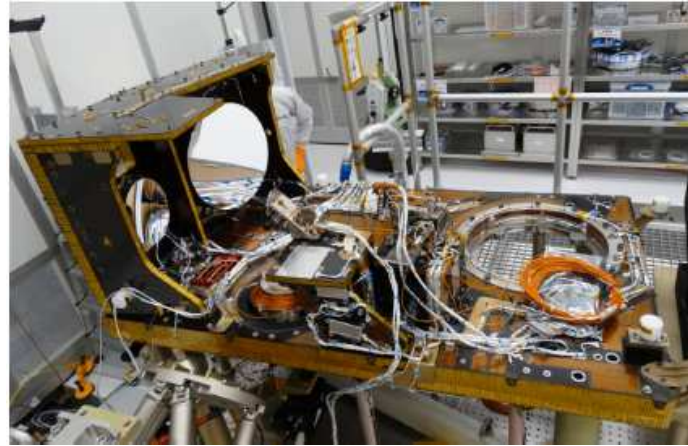


Figure 1. Flight model of the TA during alignment and before baffle mounting. The M1 and M3 mirrors are on the left.

- The light coming from the TA is then split into 5 spectral groups by a subsystem called the Spectral Separation Assembly (SSA). It is composed of a Titanium housing, in which are mounted dichroic beam-splitters, mirrors and lenses that collimate the NIR and IR spectral groups. The lenses are made of classical IR substrates such as Germanium, ZnSe, ZnS, Silicon, CaF₂, and BaF₂, all with anti-reflective coatings. The VIS spectral group is directly reflected by a mirror onto the Visible detector which is mounted on the top of the SSA housing. The WFE of the SSA ranges between 100 to 200nm for NIR/IR spectral channels.



Figure 2. View of the Spectral Separation Assembly

- The collimated IR beams then reach the cryostat, in which are mounted cold optics and NIR/IR detectors on a common cold plate. The detectors are regulated at 60K thanks to cryo-cooler. The cold optics are made of 4 separated cylindrical titanium housings (one per spectral group), in which IR lenses with anti-reflective coatings are glued. They exhibit a cold diaphragm on the top, which is conjugated with the telescope entrance pupil, and allows to limit the IR thermal emission. The cold optics are accurately mounted by pinning on the cold plate, in order to optimize co-registration performances. The goal of the cold optics is to focus the beams on the detectors. The assembly of the SSA and the cryostat is called the SSDA.



Figure 3. A cold optics housing

2. OPTICAL TESTS AT TELESCOPE LEVEL

The detailed results of optical tests at Telescope Assembly (TA) level are described in [2].

2.1 Mirror alignment and WFE measurement

One of the main integration steps of the telescope is the fine alignment of the mirrors onto the optical bench. The objective of this alignment is to achieve the specified performances in terms of WFE and line of sight. The required WFE after alignment should be lower than 100 nm rms in the whole field of view. Consequently, tolerancing analyses have shown that alignment positioning accuracies ranging from 10 μ m to 30 μ m were required depending of the mirror and alignment axis.

The mirror orientation and out-of-plane position is adjusted thanks to accurate shims, while the in-plane translations are controlled thanks to micro-metric screws for M2 most-sensitive mirror. The alignment is performed with the optical bench in horizontal position, and the gravity impact is compensated thanks to push bars under the bench. Each time a mirror is mounted, the bench deformation due to its weight is measured thanks to accurate capacitive sensors, and a force is applied to the push bars to compensate this deformation.

The WFE of the telescope is measured thanks to a Shack-Hartmann sensor which is positioned at the telescope image level. A flat auto-collimation mirror reflects the beam from the Shack-Hartmann into the telescope, and the WFE is measured in double-pass. From a first WFE measurement, a specific algorithm allows to give the required mirror displacements in order to optimize the WFE in the whole field of view. The alignment of the telescope is also described in detail in [2].

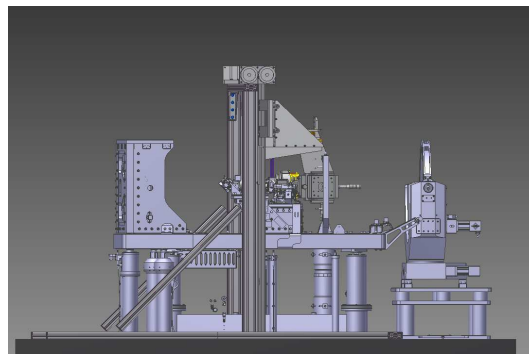


Figure 4. Illustration of telescope alignment configuration. The push bars are below the bench and the auto-collimation mirror is on the right side

The results of the WFE after alignment are given in Table 3 below in 5 points covering the center (FOV 1) and the corners of the specified field-of-view (FOV 2 to 5).

Table 3. PFM telescope alignment WFE measurement results

| FOV | Measured WFE (nm rms) | Specification (nm rms) | Status |
|-------|-----------------------|------------------------|-----------|
| FOV 1 | 40 | 100 | Compliant |
| FOV 2 | 59 | | |
| FOV 3 | 63 | | |
| FOV 4 | 49 | | |
| FOV 5 | 55 | | |

Consequently, the PFM telescope exhibits a WFE compliant and significantly better than the requirement, which will allow to save some margin at system level. The main residual aberration is astigmatism.

2.2 Focal length

Using the same Shack-Hartmann sensor as for the WFE measurement, it is also possible to measure the focal length of the telescope in the center of the field-of-view. For this purpose, 5 positions are measured along each axis, separated by 0.2mm each in the focal plane. The Shack-Hartman sensor is set to these pre-defined positions in the focal plane, and the auto-collimation mirror is adjusted to minimize the measured WFE. By measuring the lateral position of the Shack-Hartman y , and the beam angle due to the rotation of the auto-collimation mirror θ , one can derive the focal length f by using (1) valid for the center of the FOV :

$$y = f \times \tan(\theta) \quad (1)$$

The following table gives the results of the measurement, which is compliant to the requirement.

Table 4. PFM telescope paraxial focal length measurement results

| Axis | Measured focal length center FOV (mm) | Specification (mm) | Status |
|---------|---------------------------------------|--------------------|-----------|
| X (E/W) | 1647 | 1650 +/- 16mm | Compliant |
| Y (N/S) | 1659 | | |

2.3 Line of sight

The line of sight of the telescope is also checked using the Shack-Hartmann sensor positioned in the center of the focal plane. The scan mirror of the telescope is set to its reference position to point at Nadir in orbit, and the auto-collimation GSE mirror orientation is set to minimize the measured WFE. The orientation of this auto-collimation mirror then gives the line of sight of the telescope.

The requirement is that the Telescope LOS in-flight for the center of the field of view, shall be normal to the FCI mounting interface with a tolerance lower than $\pm 0.05^\circ = 180''$.

The on-ground measurement performed under ambient conditions (air at 20°C) gives a value of -23'' around X axis and 10'' around Y axis. The measurement accuracy is estimated to be in the order of 20''. The following table gives the corresponding in-flight estimation by adding the other contributors like gravity, thermo-elastic distortion and hygro-elastic stability, which were established by analyses. Since those items are deterministic a linear sum is performed. The worst case thermo-elastic effect along the orbit is selected. The telescope LOS is compliant to the requirement and exhibits significant margin.

Table 5. PFM telescope line of sight results

| Axis | LOS X (arcsec) | LOS Y (arcsec) |
|----------------|----------------|----------------|
| Measurement | -23 | 10 |
| Gravity | 11 | -12 |
| Thermo-elastic | -19 | 12 |
| Hygro-elastic | 6 | 8 |
| Total (sum) | -25 | 18 |
| Requirement | 180 | 180 |
| Status | Compliant | Compliant |

2.4 Stray-light characterization

The purpose of stray-light characterization tests performed at telescope level is to validate the scattering modeling of the mirrors. Indeed, since the satellite is operating from geostationary orbit, between 22h30 and 1h30 the Sun can illuminate the M0 and M1 mirror directly, thus generating stray-light. This stray-light will be corrected thanks to image processing algorithm, based on BRDF models of the mirrors. It is therefore necessary to check the validity of these models.

The measurement principle is to use a collimated light source at 565 nm and 880nm, and to illuminate the full telescope pupil. These two wavelengths were selected because the scattering effects are higher in the visible, so the measurement accuracy is better. It also matches the detector sensitivity range which is placed in the telescope focal plane. The instrument is mounted on a rotating stage and is illuminated out of the field of view for the following angles along NS and EW axes: 1°, 3°, 5°, 9°, 15° and 18° (up to solar baffle rejection angle). For each angular source orientation and each wavelength, the signal on all the detector pixels is recorded. The average of the stray-light on the detector matrix is taken into account for the measurement results. The stray-light level is expressed in relative irradiance with respect to a direct illumination in the field of view which is used for normalization.



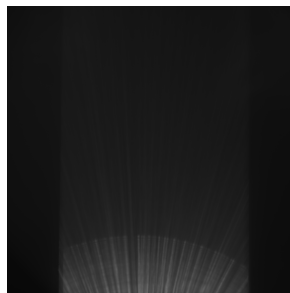
Figure 5. Stray-light measurement facility preparation – collimator (left) – rotating stage for the instrument (right)

The success criteria is that for all angles lower than 9° with respect to the LOS, the difference between measurement and test predictions shall be lower than the sum of measurement accuracy and prediction accuracy. The prediction accuracy is evaluated to be around 150%, which is classical for stray-light estimation. The test prediction is performed using the mirror BRDF models and the measured particulate contamination on witness samples. These contamination levels at the time of the measurement are given in the table below. An example of image measured is also given.

Table 6. Mirror particulate contamination level at the time of the stray-light test

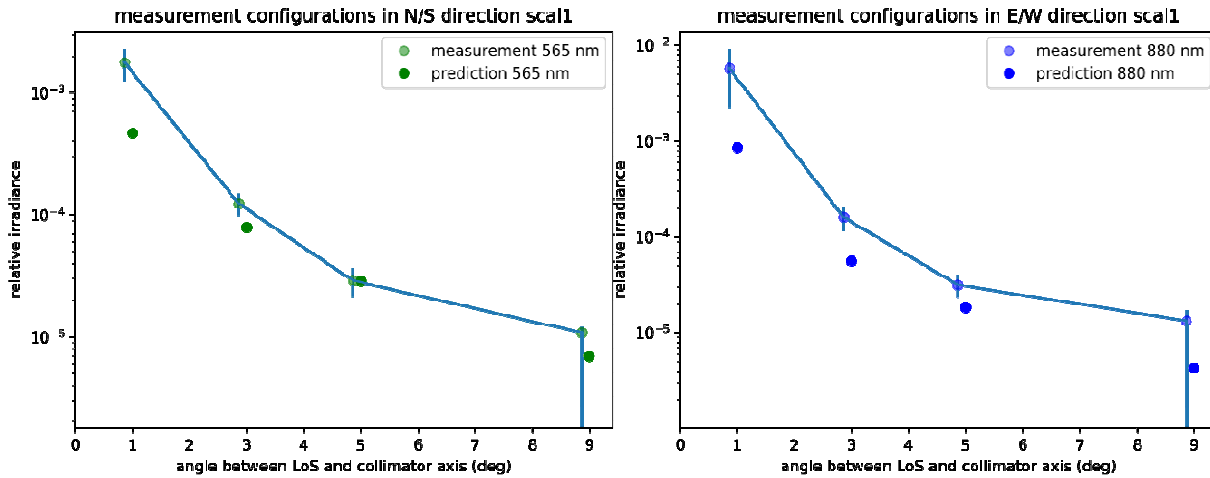
| Mirror | Contamination level (ppm) |
|--------|---------------------------|
| M0 | 178 |
| M1 | 116 |

Figure 6. Image obtained on the camera for 1° illumination angle



The results obtained are shown in the following figure for both measured wavelengths. The prediction error bar is represented by a shaded color, and the measurement error is represented by a bar around the measured stray-light irradiance value. We can notice that for both wavelengths and all angles, the measurement and prediction lie within the sum of uncertainties. This validates the BRDF models that will be used for stray-light correction.

Figure 7. TA PFM stray-light measurement results



3. OPTICAL TESTS AT SSDA LEVEL

The SSDA assembly composed of the SSA and the cryostat (containing the cold optics and NIR/IR detectors), has been tested separately by Thales Alenia Space in Cannes facilities. The optical measurement results are presented in the following paragraphs. All the tests were performed under ambient conditions, and using an Optical Ground Support Equipment (OGSE) called the GICS. This OGSE is mainly constituted by a VIS-NIR source and a black-body, and a Cassegrain telescope. These items are mounted on an hexapod to accurately control its movements. The following figure shows a picture of the GICS in the measurement configuration.

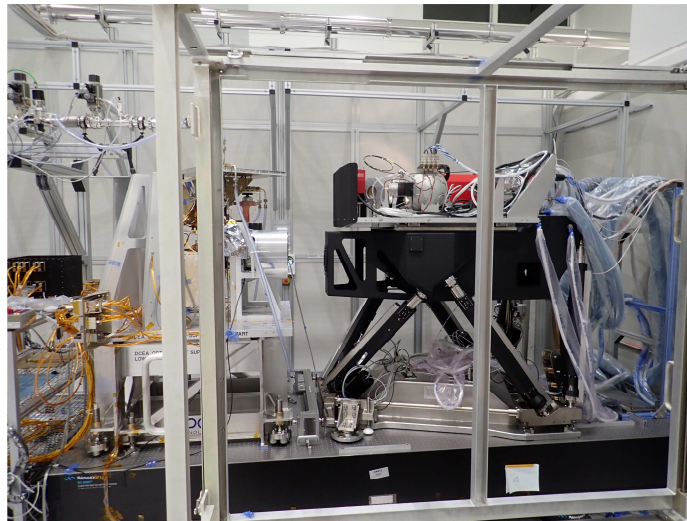


Figure 8. The GICS (on the right) in front of the SSDA

The SSDA radiometric test results are presented in [4].

3.1 MTF measurements

First, the IR detectors are adjusted in focus to typically $\pm 10\mu\text{m}$ thanks to accurate shims in order to fulfill image quality requirements. Once the shims are mounted, a MTF verification is performed using the GICS. The measurement is done on one point in the FOV of each spectral channel, to check the correct focus setting. The method of measurement is the scanning of a pixel by the image of a knife-edge. The MTF is then classically obtained by derivation and Fourier transformation of the measured signal on the pixel. The measurement accuracy is estimated to be lower than ± 0.03 at frequencies of interest.

The SSDA MTF expected values are calculated taking into account the SSA and cold optics measured WFE and the detector measured MTF by the sub-contractors. An uncertainty on this prediction, dominated by detector MTF measurement accuracy, is associated to this predicted value. On the other hand, the measured SSDA MTF value is corrected from the OGSE contribution, in particular its central obscuration. The success criterion is that the difference between the measured MTF at both relative spatial frequencies 0.42 and 0.54 (after correction) and the expected MTF, is lower than the sum of measurement and prediction uncertainties.

All measurement on both axes were measured in accordance with predicted values, except on IR1 HR 3.8 channel along X axis at 0.42 normalized spatial frequency. Actually the measured MTF value is higher than expected, thus it cannot induce any non-compliance with respect to image quality requirements. It is suspected that the expected value is underestimated since the measurement at detector level is more noisy because of the small size of the high resolution pixels.

The following figure shows an example of measured MTF on VIS 0.4 spectral channel, in function of spatial frequency. The detector cut-off frequency can clearly be seen as expected at 20 mm⁻¹. At the two frequencies of interest, the measured values are represented by a circle, while expected values are represented by a star.

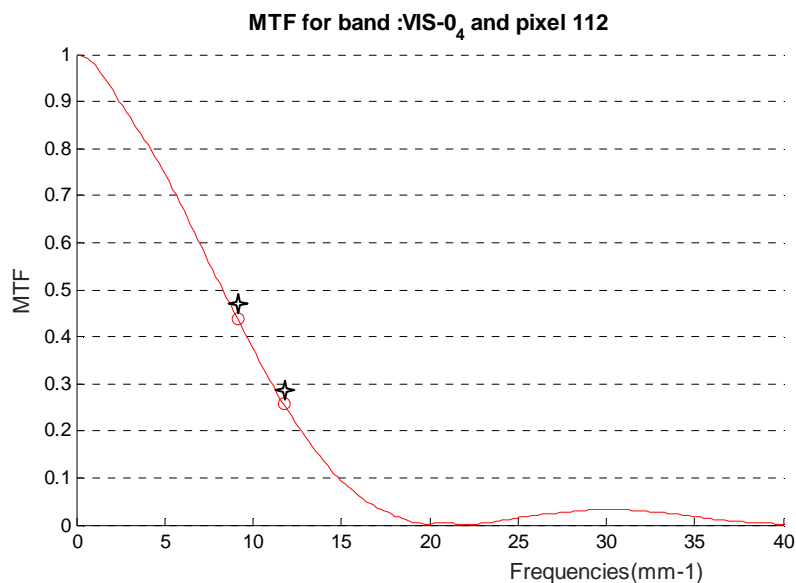


Figure 9. Example of measured MTF curve for VIS 0.4 spectral channel along X axis

3.2 Co-registration measurements

Together with MTF measurements and using the same knife-edge method, it is possible to check the co-registration of the different spectral channels. It is sufficient to check it at SSDA level since the telescope will only have a common impact on the LOS but not a relative one between spectral channels. It is required that the maximum LOS difference between any two spectral channels along the North-South axis (perpendicular to the scanning direction) is lower than 592 μm , this value being expressed in the telescope image plane. This need is ensured by design since the detectors are accurately pinned together with their corresponding cold optics lenses on the cryostat cold plate. The requirement applies only along the North-South axis because it comes from a need that each point on-ground need to be scanned by all spectral channels during the same swath, for temporal registration purposes.

The co-registration measurement results are shown in the following table. They are fully compliant to the requirement with significant margin.

Table 8. SSDA PFM co-registration measurement results

| | deregistration wrt O OBA along Y OBA (μm) in intermediate focal plane |
|-------------------------|---|
| VIS 0.4 | 120,3 |
| VIS 0.5 | 119,2 |
| VIS 0.6 | 176,3 |
| VIS 0.8 | 107,9 |
| VIS 0.9 | 106,7 |
| NIR 1.3 | 147,8 |
| NIR 1.6 | 137,8 |
| NIR 2.2 | 133,9 |
| IR1 3.8 | 68,6 |
| IR1 6.3 | 37,3 |
| IR1 7.3 | 23,4 |
| IR2 8.7 | 229,3 |
| IR2 9.7 | 221,5 |
| IR3 10.5 | 156,5 |
| IR3 12.3 | 152,5 |
| IR3 13.3 | 157,1 |
| Max difference | 205,9 |
| success criteria | 592 |

3.3 Polarization

The polarization ratio of the SSDA is measured with the GICS in the VIS and NIR spectral channels by using a polarizer in the exit pupil of the GICS rotated from 0° to 180° by steps of 5°. There is no polarization requirement for IR spectral channels. For each polarizer position the signal on the detector is recorded. If S_{min} is the minimum signal and S_{max} the maximum signal when the polarizer is rotated from 0° to 180°, the polarization ratio is assessed using (2) :

$$P = \frac{S_{max} - S_{min}}{S_{max} + S_{min}} \quad (2)$$

The measurements are performed on 3 points in the field of view of each spectral channel, to account for potential impacts of angle of incidence on optical coatings. A specific calibration of the GICS polarization ratio was performed thanks to a spectrometer, and this is subtracted from the measured values. The figure below gives an example of GICS polarization calibration curve :

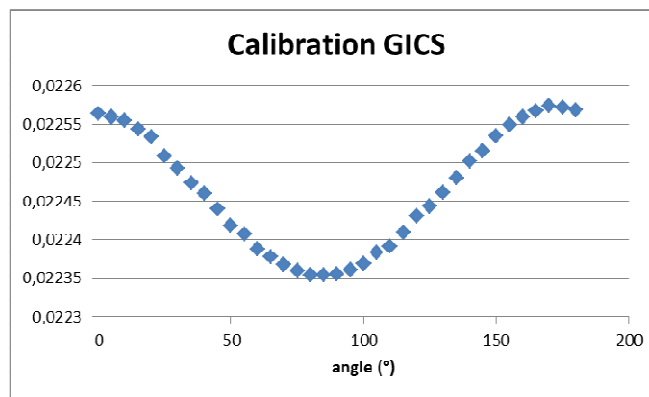


Figure 10. GICS polarization calibration for VIS 0.5 spectral channel

The measurement accuracy is estimated lower than 0.5% on the polarization ratio.

The maximum measured polarization ratio of the SSDA over all spectral channels is 1%, for a success criteria between 1.2% (VIS channels) and 2.7% (NIR channels). The measurement results are then fully compliant to the success criteria, with significant margin in the NIR.

3.4 Stray-light characterization

Because of the presence of cold optics in front of the infra-red detectors, some ghost images are formed by double-reflections on detector filters and cold optics lens surfaces. Even if the anti-reflective coatings have been designed to minimize this effect by having typical reflectivity's lower than 0.5% in the spectral range of interest, it is necessary to perform in-flight image processing to correct from this stray-light.

Stray-light simulations have been performed in order to obtain the geometrical parameters for the ghost modeling. But in order to have accurate radiometric correction of this stray-light, it is required to perform a characterization test in order to correlate the simulation with the measurement. This is due to the uncertainty on the lens measured reflectivity.

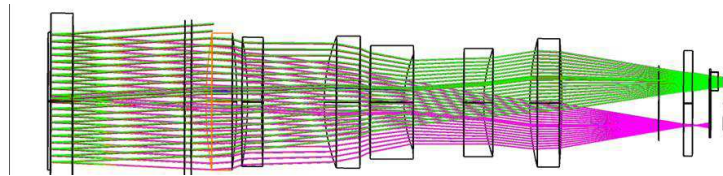


Figure 11. Example of stray-light simulation with illustration of a ghost path in green

The stray-light correction being based on the convolution of the image with a PSF, it is necessary to simulate and measure ghost images produced by a point source. In this configuration, the level of irradiance of the ghost image to be measured can be as low as 10^{-5} to 10^{-6} with respect to the point source direct image signal. It is therefore necessary to perform the measurement with a very powerful source, like the hot black-body which is available in the GICS (1200°C). In order to meet stray-light needs after correction, a measurement accuracy of 15% on the ghost irradiance is required, which is very challenging due to its low level. So in the far IR spectral range, specific precautions were applied to perform background acquisitions in the same configuration than the stray-light acquisition. These background levels were then subtracted to the ghost irradiance acquisition, in order to fulfill this accuracy. It is also necessary to measure the variation of the ghost signal in the field of view, so the measurement was performed for 25 positions on each infra-red detector, as illustrated by the figure below where the channels are in yellow and measurement points in black :

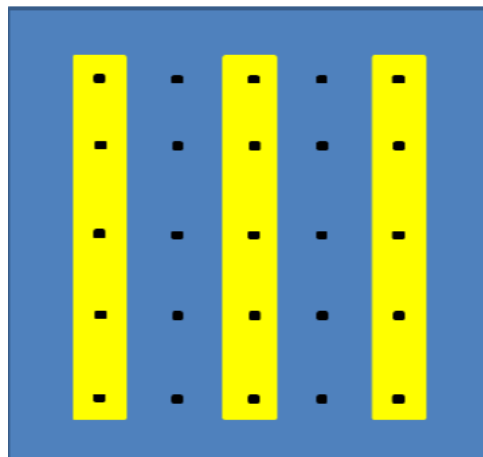


Figure 12. PSF positions for SSDA stray-light characterization

The measurement results show that all the ghost images are at the expected location and with the correct size. There is no unexpected stray-light path found in the measurement. This test is a characterization so there is no success criterion. The following figure shows an example of simulation results compared with measurement for the NIR 1.3 spectral channel. We can notice that the measured location and radiometric signal of the ghost image are consistent with simulated values. In the figure below the slight difference in ghost position comes from the fact that simulated pixel and measured pixel were not perfectly identical during test.

This characterization test will allow to tune the ghost model, in order to feed the stray-light correction algorithm. This stray-light correction is expected to lower the stray-light of the raw images by a factor of about 3.

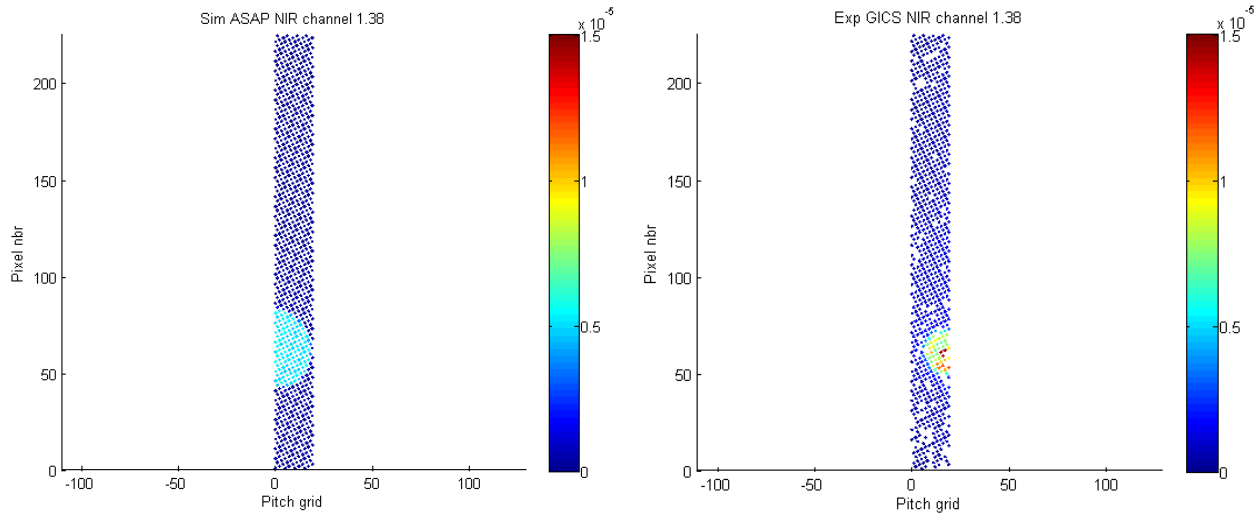


Figure 13. SSDA stray-light measurement example for channel NIR 1.3

4. CONCLUSION AND PERSPECTIVES

We have presented the optical tests principle and results performed on the two sub-systems of the FCI , the telescope and the objective and detection assembly called SSDA. All the optical test results are compliant with respect to the success criteria. In particular the telescope WFE, focal length and line of sight as well as the SSDA MTF, co-registration, and polarization are fully meeting the performance needs. Additionally, stray-light for both telescope and SSDA have been characterized on-ground in order to provide the inputs necessary for in-orbit image correction algorithms.

During the first half of 2020, these two successfully tested sub-systems were integrated together to build the FCI PFM, which will undergo optical vacuum testing at the timeframe of beginning 2021. The FCI PFM will then be delivered to the MTG satellite. It will provide full images of the Earth to allow accurate prediction of meteorological phenomena and climate monitoring.

ACKNOWLEDGMENTS

The authors would like to thank ESA for their full support, as well as all MTG sub-contractors, in particular OHB for their constant work all along this development.

REFERENCES

- [1] Ouaknine J. et al, "The FCI on board MTG : optical design and performances", ICSO proceedings, 2014
- [2] Fray S. et al, "First Flight model Optical performance test on the Flexible Combined Imager Telescope Assembly of Meteosat Third Generation", ICSO 2020
- [3] Martin P. et al, "FCI instrument on-board MeteoSat Third Generation Satellite - design and development status", ICSO 2020
- [4] Gardette H. et al, "Meteosat Third Generation : presentation of the video detection chains", ICSO 2020